Solving the Quantum Many-Body Problem via Correlations Measured with a Momentum Microscope

S. S. Hodgman,[1,*] R. I. Khakimov,[1] R. J. Lewis-Swan,[2,3] A. G. Truscott,[1] and K. V. Kheruntsyan[2]
[1]Research School of Physics and Engineering, Australian National University, Canberra 0200, Australia
[2]University of Queensland, School of Mathematics and Physics, Brisbane, Queensland 4072, Australia
[3]JILA, NIST and Department of Physics, University of Colorado, 440 UCB Boulder, Colorado 80309, USA
(Received 10 April 2017; published 14 June 2017)

In quantum many-body theory, all physical observables are described in terms of correlation functions between particle creation or annihilation operators. Measurement of such correlation functions can therefore be regarded as an operational solution to the quantum many-body problem. Here, we demonstrate this paradigm by measuring multiparticle momentum correlations up to third order between ultracold helium atoms in an s-wave scattering halo of colliding Bose-Einstein condensates, using a quantum many-body momentum microscope. Our measurements allow us to extract a key building block of all higher-order correlations in this system—the pairing field amplitude. In addition, we demonstrate a record violation of the classical Cauchy-Schwarz inequality for correlated atom pairs and triples. Measuring multiparticle momentum correlations could provide new insights into effects such as unconventional superconductivity and many-body localization.

DOI: 10.1103/PhysRevLett.118.240402

In quantum physics, fully understanding and characterizing complex systems, comprising a large (often macroscopic) number of interacting particles, is an extremely challenging problem. Solutions within the standard framework of (first-quantized) quantum mechanics generally require the knowledge of the full quantum many-body wave function. This necessitates an exponentially large amount of information to be encoded and simulated using the many-body Schrödinger equation. In an equivalent (second-quantized) quantum field theory formulation, the fundamental understanding of quantum many-body systems comes through the description of all physical observables via correlation functions between particle creation and annihilation operators. Here, the exponential complexity of the quantum many-body problem is converted into the need to know all possible multiparticle correlation functions, starting from two-, three-, and increasing to arbitrary N-particle (or higher-order) correlations.

From an experimental viewpoint, an operational solution to the quantum many-body problem is therefore equivalent to measuring all multiparticle correlations. In certain cases, however, knowing only a specific set of (few-body or lower-order) correlations is sufficient to allow a solution of the many-body problem to be constructed. This was recently shown for phase correlations between two coupled one-dimensional (1D) Bose gases [1]. Apart from facilitating the description of physical observables, characterizing multiparticle correlations is important for introducing controlled approximations in many-body physics, such as the virial- and related cluster-expansion approaches that rely on truncation of the Bogolyubov-Born-Green-Kirkwood-Yvon hierarchy [2,3]. Momentum correlations up to sixth order [4] and phase correlations up to eighth [1] and tenth order [5] have so far been measured in ultracold atomic gases. More generally, multiparticle correlation functions have been used to experimentally characterize the fundamental properties of various systems, such as thermal Bose and Fermi gases [6], weakly and strongly interacting 1D Bose gases [7–9], tunnel-coupled 1D tubes [1,5], collision halos [10–12], and phenomena such as prethermalization [13] and transverse condensation [14]. Correlations between multiple photons are also routinely used in numerous quantum optics experiments including ghost imaging [15,16], defining criteria for nonclassicality [17,18], analyzing entangled states generated by parametric down conversion [19], and characterizing single photon sources [20].

Here, we demonstrate an experimental solution of the many-body problem as outlined above by measuring second- and third-order correlations between momentum-correlated atoms in a collisional halo between two Bose-Einstein condensates (BECs). The halo is generated by spontaneous s-wave scattering of two colliding BECs [10,12,21], creating a spherical shell of pair-correlated atoms (see Fig. 1). After a time-of-flight expansion, we detect the positions of individual atoms, which are mapped back to the initial momenta of the atoms directly after the collision [47]. This means that we reconstruct momentum correlation functions from the momenta of individual atoms with full 3D resolution. Thus, our detector setup can be regarded as a *quantum many-body momentum microscope*, complementary to the quantum gas *in situ* microscopes created using optical lattices [48–53] or arrays of optical tweezers [54]. We characterize and compare all possible

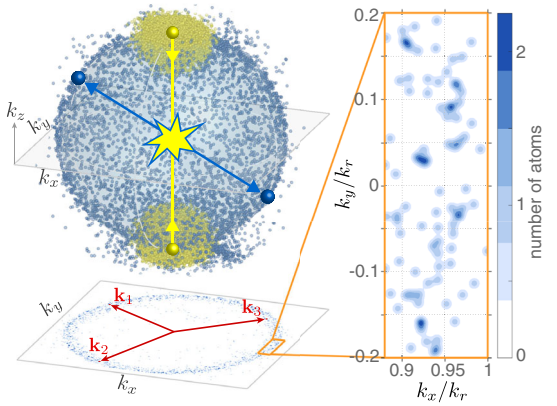

FIG. 1. *Atomic momenta as measured by the quantum many-body momentum microscope.* Individual momenta of detected atoms are reconstructed in 3D momentum space, with the main image showing the collision halo, with dense (yellow) patches on the north and south poles showing unscattered atoms from the pair of colliding condensates. The highlighted balls and arrows are an illustration of the underlying microscopic interactions—the binary s-wave collisions. The 2D histograms below show an equatorial slice through the experimental data, where the red arrows $\mathbf{k}_1$, $\mathbf{k}_2$, and $\mathbf{k}_3$ indicate three arbitrarily chosen momenta for which, e.g., three-atom correlations can be analyzed via coincidence counts. Experimental data from ten runs is shown, which approximates the density present in a single halo, given our detection efficiency of ~10%. Individual atoms can be seen in the magnified inset, represented as 2D Gaussians with a width equal to the detector resolution. The size of the balls representing the individual atoms on the main 3D image are not to scale.

back-to-back and collinear atomic correlation functions for two and three atoms, showing the relationship between the different correlation functions and demonstrating a record violation of the classical Cauchy-Schwarz inequality between the peak values of correlation functions.

The experiments start with a BEC of $\sim 10^6$ ^{4}He* atoms magnetically trapped in the $m_J = +1$ sublevel of the long lived metastable (2^3S_1) state [55]. The s-wave scattering halos of correlated pairs are produced *via* a two-step process. First, we transfer ~95% of the BEC atoms to the untrapped $m_J = 0$ sublevel with a Raman pulse, giving the atoms a downward (i.e., along the $\hat{\mathbf{z}}$ direction) momentum of $\mathbf{K} = -\sqrt{2}k_0\hat{\mathbf{z}}$ [21] in wave number units, where $k_0 = 2\pi/\lambda$ and $\lambda = 1083.2$ nm is the wavelength of a diffraction photon. The untrapped BEC is then diffracted using a second pulse into two or more diffraction orders, using either Bragg or Kapitza-Dirac diffraction [21]. Adjacent pairs of diffracted condensates then collide, producing spherical halos of spontaneously scattered atom pairs via s-wave collisions [10]. Each halo has a radius in momentum space of $k_r \approx k_0/\sqrt{2}$ and a radial Gaussian width of $w \approx 0.03k_r$. The average mode occupancy in each halo ranges from $n = 0.0017(17)$ to $n = 0.44(2)$. As the scattering in our experiment is always in the spontaneous pair-production regime [21], the scattering halo can be approximated by an overall quantum many-body state that is the product of independent two-mode squeezed vacuum states analogous to those produced by parametric down-conversion in quantum optics.

The expanding halos then fall ~850 mm (time of flight [TOF] ~416 ms) onto a multichannel plate and delay-line detector. Because of the 19.8 eV internal energy of the 2^3S_1 state, the individual positions of atoms can be reconstructed in 3D, with a spatial resolution of ~120 μm in x, y (momentum resolution $\sim 0.0044k_r$) and a temporal resolution along z of ~2 ns ($\equiv$8 nm or $3 \times 10^{-7}k_r$). As we are interested in correlations between atoms in different momentum modes, we convert position and time to momentum centered on each halo [21].

From the reconstructed momentum for each atom, we construct various momentum correlation functions from coincidence counts between atoms within each experimental run that are averaged over all runs [21]. First, we look at momentum correlations between three atoms with momenta $\mathbf{k}_3$, $\mathbf{k}_1 = -\mathbf{k}_3 + \Delta\mathbf{k}_1$, and $\mathbf{k}_2 = -\mathbf{k}_3 + \Delta\mathbf{k}_2$, i.e., the second two atoms on the opposite side of the halo to the first [see Figs. 2(a)–2(c) for illustration]. We define the relevant correlation function as $\bar{g}^{(3)}_{BB}(\Delta k_1, \Delta k_2)$ and refer to it as back-to-back (BB), which is averaged with respect to $\mathbf{k}_3$ over the halo and spherically integrated with respect to the directions of vectors $\Delta\mathbf{k}_1$ and $\Delta\mathbf{k}_2$. Thus, it is a function of the absolute values $\Delta k_1 = |\Delta\mathbf{k}_1|$ and $\Delta k_2 = |\Delta\mathbf{k}_2|$ [21].

Figure 2(g) shows a typical surface plot of $\bar{g}^{(3)}_{BB}(\Delta k_1, \Delta k_2)$ for the s-wave halo generated by Kapitza-Dirac orders $l = (-2, -3)$. This surface plot also contains other many-body correlation functions within it, shown schematically in Figs. 2(a)–2(c). When $\Delta k_2 = 0$, we can plot $\bar{g}^{(3)}_{BB}(\Delta k_1, 0)$ [red line in Fig. 2(g)], which will asymptotically approach $\bar{g}^{(2)}_{BB}(0)$—the two-particle correlation function with one atom on each side of the halo—for $\Delta k_1 \gg \sigma_{BB}$, where σ_{BB} is the two-particle back-to-back correlation length. Taking $\Delta k_2 \gg \sigma_{BB}$, we can also plot $\bar{g}^{(3)}_{BB}(\Delta k_1, \Delta k_2 \gg \sigma_{BB})$ (blue line), which is equivalent to $\bar{g}^{(2)}_{BB}(\Delta k_1)$ and approaches the uncorrelated case of $\bar{g}^{(2)}_{BB}(\Delta k_1 \gg \sigma_{BB}) = 1$ for large values of Δk_1 (see [21] for a full discussion of the relationship between various correlation functions).

We also measure the collinear (CL) three-atom correlation function [shown in Figs. 2(d)–2(f)], defined analogously as $\bar{g}^{(3)}_{CL}(\Delta k_1, \Delta k_2)$, where now $\Delta k_1 = |\mathbf{k}_3 - \mathbf{k}_1|$ and $\Delta k_2 = |\mathbf{k}_3 - \mathbf{k}_2|$. A surface plot of this function, measured for the Bragg halo with maximum mode occupancy, is shown in Fig. 2(h). Like $\bar{g}^{(3)}_{BB}(\Delta k_1, \Delta k_2)$, this full correlation function also contains other many-body correlations: for example, $\bar{g}^{(3)}_{CL}(\Delta k_1, 0)$ [red line in Fig. 2(h)] will asymptotically approach $\bar{g}^{(2)}_{CL}(0)$ (the two-atom collinear

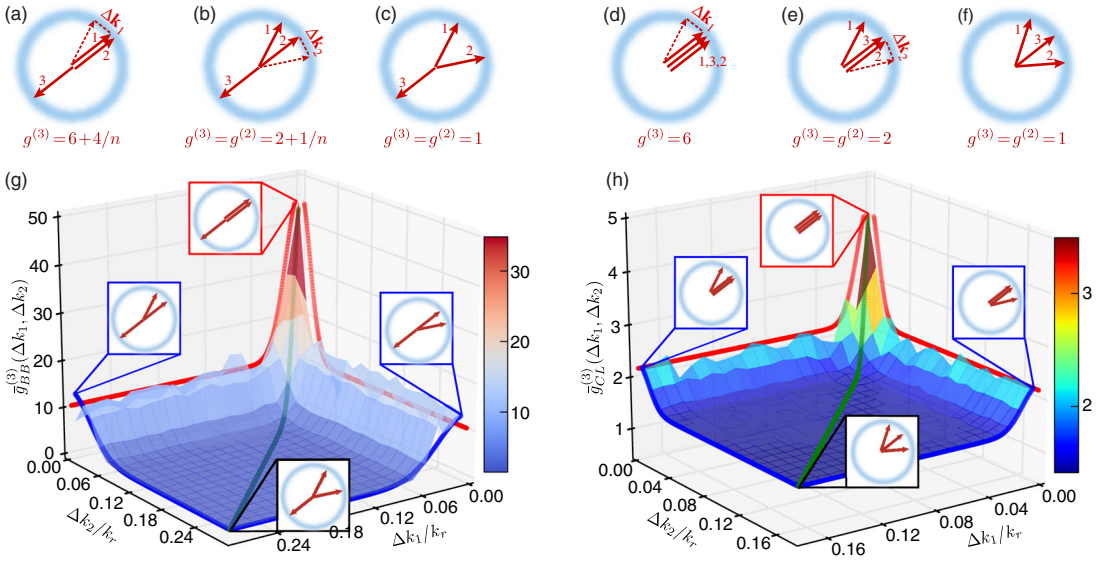

FIG. 2. *Three-body momentum correlation functions*. The various back-to-back (a)–(c) and collinear (d)–(f) correlation functions between three atoms in the scattering halo, with the maximum expected value of each correlation function indicated. (g) Surface plot showing the correlation function between two collinear and one back-to-back atom $\bar{g}^{(3)}_{BB}(\Delta k_1,\Delta k_2)$ is shown for the s-wave halo that has a mean occupation of $n=0.010(5)$ atoms per mode. The red and blue solid lines show cases (a) and (b), respectively [21], while the green solid line is the 1D Gaussian fit used to extract $\bar{g}^{(3)}_{BB}(0,0)$. (h) The correlation function between three collinear atoms $\bar{g}^{(3)}_{CL}(\Delta k_1,\Delta k_2)$ is shown for the s-wave halo with $n=0.44(2)$. The red and blue solid lines show cases (d) and (e), respectively, while the green solid line is the 1D Gaussian fit used to extract $\bar{g}^{(3)}_{CL}(0,0)$ [21]. Insets show visual representations of the relevant cases at four selected points on each plot.

correlation function), while $\bar{g}^{(3)}_{CL}(\Delta k_1,\Delta k_2\gg\sigma_{CL})$ (blue line) will yield $\bar{g}^{(2)}_{CL}(\Delta k_1)$ [21]. Figures 2(g) and 2(h) therefore show a full characterization of the hierarchy of all three-body and two-body correlation functions present in our system.

Our collisional halo is an example of a quantum many-body system which, in the spontaneous scattering regime, satisfies Wick's factorization scheme [21]. This requires knowledge of both the normal and anomalous second-order operator moments in momentum space, $n_{\mathbf{k},\mathbf{k}+\Delta\mathbf{k}}=\langle\hat{a}^\dagger_{\mathbf{k}}\hat{a}_{\mathbf{k}+\Delta\mathbf{k}}\rangle$ and $m_{\mathbf{k},-\mathbf{k}+\Delta\mathbf{k}}=\langle\hat{a}_{\mathbf{k}}\hat{a}_{-\mathbf{k}+\Delta\mathbf{k}}\rangle$, with $\hat{a}^\dagger_{\mathbf{k}}$ and $\hat{a}_{\mathbf{k}}$ being the respective mode creation and annihilation operators, and the diagonal element of $n_{\mathbf{k},\mathbf{k}+\Delta\mathbf{k}}$ giving the average mode occupancy $n_{\mathbf{k}}\equiv n_{\mathbf{k},\mathbf{k}}$. Knowledge of these quantities is sufficient to reconstruct all higher-order correlation functions and thus, completely solve the many-body problem for our system. Here, the anomalous occupancy $m_{\mathbf{k}}\equiv m_{\mathbf{k},-\mathbf{k}}$ (related to the anomalous Green's function in quantum field theory) describes the pairing field amplitude between atoms with equal but opposite momenta and is similar to the expectation value of the Cooper pair operator in the Bardeen-Cooper-Schrieffer theory of superconductivity, although in our case, the pairing is between two identical bosons.

To examine these factorization properties further, we analyze the dependence of peak correlation amplitudes on the peak halo mode occupancy $n_{\mathbf{k}_0}$ and compare them with theoretical predictions. The theory relies on the relationship between the peak anomalous occupancy $|m_{\mathbf{k}_0}|$ and $n_{\mathbf{k}_0}$: $|m_{\mathbf{k}_0}|^2=n_{\mathbf{k}_0}(n_{\mathbf{k}_0}+1)$ [21]. In Fig. 3(a), we plot the measured peak back-to-back correlation amplitude between two-atoms $\bar{g}^{(2)}_{BB}(0)$, for values of average mode occupancy $n\simeq n_{\mathbf{k}_0}$ that span more than 2 orders of magnitude. $\bar{g}^{(2)}_{BB}(0)$ is extracted by fitting $\bar{g}^{(2)}_{BB}(\Delta k)$ with a Gaussian (for details and plots, see [21]). From analytic theory, we expect $\bar{g}^{(2)}_{BB}(0)$ to scale with n as [21]

$$\bar{g}^{(2)}_{BB}(0)=(n^2_{\mathbf{k}_0}+|m_{\mathbf{k}_0}|^2)/n^2_{\mathbf{k}_0}\simeq 2+1/n. \qquad (1)$$

This relation is plotted as the dashed line in Fig. 3(a), which matches the data well considering that it is a no free parameters fit. For comparison, we also plot the peak collinear correlation between two atoms, $\bar{g}^{(2)}_{CL}(0)$, shown by squares in Fig. 3(a) and extracted from $\bar{g}^{(2)}_{CL}(\Delta k)$ in the same way as $\bar{g}^{(2)}_{BB}(0)$. We see values of $\bar{g}^{(2)}_{CL}(0)\simeq 1.5$, seemingly independent of the mode occupancy. This trend is expected theoretically, although in the limit of perfect resolution, we would expect $\bar{g}^{(2)}_{CL}(0)=2$ (as in the Hanbury Brown–Twiss effect [10,56]) for all values of n.

From the measured $\bar{g}^{(2)}_{BB}(0)$ and $\bar{g}^{(2)}_{CL}(0)$ at each n, we are able to extract the key nontrivial component of all higher-order correlations in the scattering halo—the absolute value of the average anomalous occupancy $|m|\simeq|m_{\mathbf{k}_0}|$. This is

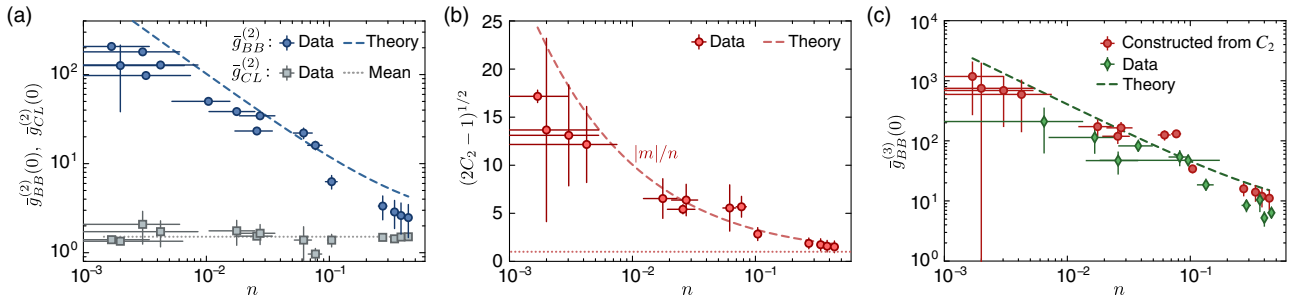

FIG. 3. *Peak two- and three-atom correlation amplitudes and anomalous occupancy $|m|$ vs halo mode occupancy n.* (a) The measured peak two-atom back-to-back and collinear correlation amplitudes $\bar{g}^{(2)}_{BB}(0)$ (blue circles) and $\bar{g}^{(2)}_{CL}(0)$ (grey squares), respectively, plotted against the average halo mode occupancy (n) for different halos. The dashed (blue) line shows the analytic prediction of Eq. (1). We expect theoretically that $\bar{g}^{(2)}_{CL}(0) = 2$ for all n, but due to the finite resolution of the detector and the bins used to calculate the correlation function, this is reduced slightly. The dotted line shows the mean value of $\bar{g}^{(2)}_{CL}(0)$. (b) The quantity $(2C_2 - 1)^{1/2} \simeq |m|/n$ [where $C_2 \equiv \bar{g}^{(2)}_{BB}(0)/\bar{g}^{(2)}_{CL}(0)$], with $|m|$ the anomalous occupancy, is plotted against n along with the theoretical prediction (dashed red line) of $|m|/n = (1 + 1/n)^{1/2}$. The horizontal dotted line at unity is drawn for reference, showing that $|m| > n$ for all our data points. (c) $\bar{g}^{(3)}_{BB}(0, 0)$ vs n, with green diamonds showing experimental data [extracted from fits to $\bar{g}^{(3)}_{BB}(\Delta k, \Delta k)$, as shown by the green line in Fig. 2(g)] and the dashed line showing the theoretical prediction of Eq. (2). Red circles are reconstructed using experimental data for C_2. Error bars for all three plots show the combined statistical and fit uncertainties [21].

found through the relation $|m_{\mathbf{k}_0}|^2/n^2_{\mathbf{k}_0} = 2C_2 - 1$, where $C_2 \equiv \bar{g}^{(2)}_{BB}(0)/\bar{g}^{(2)}_{CL}(0)$. Using the data of Fig. 3(a) to calculate C_2, we plot $(2C_2 - 1)^{1/2} \simeq |m|/n$ in Fig. 3(b). A value of $|m| > n$ is necessary for any system to exhibit nonclassical (quantum) behavior, such as two-mode quadrature squeezing, Einstein-Podolsky-Rosen quadrature-entanglement [57], and Bell inequality violation [58]. The fact that we measure values of $|m|/n > 1$ for all n (with $|m|/n \gg 1$ for smallest n) is a further demonstration of the strong quantum nature of our system. Since all order correlation functions for this system can be expressed as a function of n and $|m|$, measuring these parameters is essentially equivalent to solving the many-body problem for the collisional halo.

Following a similar analysis for the peak three-atom back-to-back correlation amplitude [21], extracting $\bar{g}^{(3)}_{BB}(0, 0)$ from Gaussian fits to $\bar{g}^{(3)}_{BB}(\Delta k, \Delta k)$, we plot these peak values as a function of n in Fig. 3(c). Theoretically, we expect $\bar{g}^{(3)}_{BB}(0, 0)$ to scale with $|m|$ and n as [21]

$$\bar{g}^{(3)}_{BB}(0, 0) = (2n^3_{\mathbf{k}_0} + 4n_{\mathbf{k}_0}|m_{\mathbf{k}_0}|^2)/n^3_{\mathbf{k}_0} \simeq 6 + 4/n. \quad (2)$$

This reflects the enhancement in the correlation amplitude due to both the back-to-back and collinear correlations [21]. In Fig. 3(c), we plot Eq. (2) as a dashed green line, which agrees quite well with the experimental data.

Additionally, we can construct $\bar{g}^{(3)}_{BB}(0, 0)$ from our measured values of C_2, through the relation $\bar{g}^{(3)}_{BB}(0, 0) = 8C_2 - 2$. We plot these values in Fig. 3(c), which match the theory well. This is a direct demonstration of how lower-order correlation functions can be used to construct higher-order correlation functions, showing that measuring a finite number of correlation functions can be operationally equivalent to solving the many-body problem.

The low probability associated with four or more atom coincidence events means that we are unable to perform a full, quantitative analysis of the hierarchy of fourth- and higher-order correlation functions. However, we are able to measure the back-to-back correlation function $\bar{g}^{(4)}_{BB}(\Delta k_1, \Delta k_2, \Delta k_3)$ for four atoms, two on each opposite side of the halo [21], for $n = 0.31(12)$. This yields $\bar{g}^{(4)}_{BB}(0, 0, 0) = 70(40)$, compared to the theoretically expected value of $\bar{g}^{(4)}_{BB}(0,0,0) \simeq 24 + 24/n + 4/n^2 \simeq 143$ for this mode occupancy [21].

An important feature of our BEC collision experiments compared to previous work [10,11] is that we are able to explore a much larger parameter space, including relatively low values of n and small correlation lengths [21]. Because of this, the values of $\bar{g}^{(2)}_{BB}(0)$ that we measure greatly exceed the maximum possible collinear correlation value of $\bar{g}^{(2)}_{CL}(0) = 2$. Thus our results are the first measurements in the regime $\bar{g}^{(2)}_{BB}(0) \gg \bar{g}^{(2)}_{CL}(0)$. This is a violation of the simplest formulation of the Cauchy-Schwarz inequality [11] for our system, which dictates that classically, we would be restricted to $\bar{g}^{(2)}_{BB}(0) \leq \bar{g}^{(2)}_{CL}(0)$. All previous similar measurements with ultracold atoms were limited to peak correlation amplitudes $\bar{g}^{(2)}_{BB}(0) \simeq \bar{g}^{(2)}_{CL}(0)$ [10,11]. This meant that they were only able to show a violation of the Cauchy-Schwarz inequality for volume-integrated atom numbers, rather than bare peak correlations [21]. Therefore, our measurement of $\bar{g}^{(2)}_{BB}(0) \gg \bar{g}^{(2)}_{CL}(0)$, with $C_2 = \bar{g}^{(2)}_{BB}(0)/\bar{g}^{(2)}_{CL}(0) > 100$, represents a more straightforward and much stronger violation of the Cauchy-Schwarz

inequality (cf. the maximum value of the corresponding correlation coefficient $C_2 \simeq 1.2$ measured in Ref. [11]). In fact, to the best of our knowledge even for optical experiments the largest value measured is $C_2 \simeq 58$ [21,59], meaning that our result of $C_2 > 100$ is a record for any source.

The Cauchy-Schwarz inequality can also be formulated for higher-order correlation functions. For three-atom correlations in our system, it states $\bar{g}^{(3)}_{BB}(0,0) \leq (\bar{g}^{(2)}_{CL}(0))^{3/2}$ [18]. Again, we violate this inequality for all data in Fig. 3, with a maximum violation of $\simeq$100.

To summarize, we have used a quantum many-body momentum microscope to analyze the spontaneous s-wave scattering halos of correlated atom pairs with a range of halo mode occupancies n spanning over 2 orders of magnitude. We measured the third-order correlation functions $\bar{g}^{(3)}_{BB}$ and $\bar{g}^{(3)}_{CL}$ and confirmed the nontrivial many-body nature of the correlations present. Unlike previous similar measurements, we were able to extract the absolute value of the anomalous occupancy $|m|$ as a function of n. $|m|$ and n are all that is required for understanding and predicting all higher-order correlation functions in this system, hence solving the quantum many-body problem in this case. We have also demonstrated a high degree of violation of the classical Cauchy-Schwarz inequality for both two and three atom correlations. This is the first measurement for three atoms, while our two atom result beats the only previous experiment with atoms [11] by nearly 2 orders of magnitude.

This demonstrated ability to measure higher-order quantum correlations in a complex many-body system (an s-wave scattering halo) means that a momentum microscope will be a valuable tool for probing other many-body effects in quantum simulators that possess nontrivial correlations (although this may require additional considerations [21]). Such effects include many-body localisation and glassy dynamics [60], unconventional superconductivity [61], universal three-body recombination, and Efimov resonances [62]. Other possible applications include the use of such a microscope as a direct dynamical probe of nonequilibrium many-body effects in TOF expansion.

We thank I. Bloch, C. Regal, and A.-M. Rey for helpful comments and B. Henson and D. Shin for technical assistance. This work was supported through Australian Research Council (ARC) Discovery Project Grants No. DP120101390, No. DP140101763, and No. DP160102337. S. S. H. is supported by ARC Discovery Early Career Researcher Award No. DE150100315. A. G. T. is supported by ARC Future Fellowship Grant No. FT100100468.

*sean.hodgman@anu.edu.au

[1] T. Schweigler, V. Kasper, S. Erne, B. Rauer, T. Langen, T. Gasenzer, J. Berges, and J. Schmiedmayer, arXiv:1505.03126.
[2] I. Shavitt and R. J. Bartlett, *Many-Body Methods in Chemistry and Physics: MBPT and Coupled-Cluster Theory* (Cambridge University Press, Cambridge, England, 2009).
[3] M. Kira and S. W. Koch, *Semiconductor Quantum Optics* (Cambridge University Press, Cambridge, England, 2011).
[4] R. G. Dall, A. G. Manning, S. S. Hodgman, W. RuGway, K. V. Kheruntsyan, and A. G. Truscott, Nat. Phys. **9**, 341 (2013).
[5] T. Langen, S. Erne, R. Geiger, B. Rauer, T. Schweigler, M. Kuhnert, W. Rohringer, I. E. Mazets, T. Gasenzer, and J. Schmiedmayer, Science **348**, 207 (2015).
[6] T. Jeltes, J. M. McNamara, W. Hogervorst, W. Vassen, V. Krachmalnicoff, M. Schellekens, A. Perrin, H. Chang, D. Boiron, A. Aspect, and C. I. Westbrook, Nature (London) **445**, 402 (2007).
[7] T. Kinoshita, T. Wenger, and D. S. Weiss, Phys. Rev. Lett. **95**, 190406 (2005).
[8] J. Armijo, T. Jacqmin, K. V. Kheruntsyan, and I. Bouchoule, Phys. Rev. Lett. **105**, 230402 (2010).
[9] B. Fang, A. Johnson, T. Roscilde, and I. Bouchoule, Phys. Rev. Lett. **116**, 050402 (2016).
[10] A. Perrin, H. Chang, V. Krachmalnicoff, M. Schellekens, D. Boiron, A. Aspect, and C. I. Westbrook, Phys. Rev. Lett. **99**, 150405 (2007).
[11] K. V. Kheruntsyan, J.-C. Jaskula, P. Deuar, M. Bonneau, G. B. Partridge, J. Ruaudel, R. Lopes, D. Boiron, and C. I. Westbrook, Phys. Rev. Lett. **108**, 260401 (2012).
[12] R. I. Khakimov, B. M. Henson, D. K. Shin, S. S. Hodgman, R. G. Dall, K. G. H. Baldwin, and A. G. Truscott, Nature (London) **540**, 100 (2016).
[13] M. Gring, M. Kuhnert, T. Langen, T. Kitagawa, B. Rauer, M. Schreitl, I. Mazets, D. A. Smith, E. Demler, and J. Schmiedmayer, Science **337**, 1318 (2012).
[14] W. RuGway, A. G. Manning, S. S. Hodgman, R. G. Dall, A. G. Truscott, T. Lamberton, and K. V. Kheruntsyan, Phys. Rev. Lett. **111**, 093601 (2013).
[15] K. W. C. Chan, M. N. O'Sullivan, and R. W. Boyd, Opt. Lett. **34**, 3343 (2009).
[16] X.-H. Chen, I. N. Agafonov, K.-H. Luo, Q. Liu, R. Xian, M. V. Chekhova, and L.-A. Wu, Opt. Lett. **35**, 1166 (2010).
[17] W. Vogel, Phys. Rev. Lett. **100**, 013605 (2008).
[18] D.-S. Ding, W. Zhang, S. Shi, Z.-Y. Zhou, Y. Li, B.-S. Shi, and G.-C. Guo, Optica **2**, 642 (2015).
[19] F. Bussières, J. A. Slater, N. Godbout, and W. Tittel, Opt. Express **16**, 17060 (2008).
[20] A. B. U'Ren, C. Silberhorn, J. L. Ball, K. Banaszek, and I. A. Walmsley, Phys. Rev. A **72**, 021802 (2005).
[21] See Supplemental Material at http://link.aps.org/supplemental/10.1103/PhysRevLett.118.240402 for details, which includes additional Refs. [22–46].
[22] P. Ziń, J. Chwedeńczuk, A. Veitia, and K. Rzążewski, and M. Trippenbach, Phys. Rev. Lett. **94**, 200401 (2005).
[23] P. Ziń, J. Chwedeńczuk, and M. Trippenbach, Phys. Rev. A **73**, 033602 (2006).
[24] M. Ögren and K. V. Kheruntsyan, Phys. Rev. A **79**, 021606 (2009).
[25] D. F. Walls and G. J. Milburn, *Quantum Optics* (Springer Science and Business Media, New York, 2007).
[26] C. M. Savage, P. E. Schwenn, and K. V. Kheruntsyan, Phys. Rev. A **74**, 033620 (2006).

[27] R. J. Lewis-Swan and K. V. Kheruntsyan, Nat. Commun. **5**, 3752 (2014).
[28] M. Ögren and K. V. Kheruntsyan, Phys. Rev. A **82**, 013641 (2010).
[29] J. Chwedeńczuk, P. Ziń, K. Rzążewski, and M. Trippenbach, Phys. Rev. Lett. **97**, 170404 (2006).
[30] P. Deuar and P. D. Drummond, Phys. Rev. Lett. **98**, 120402 (2007).
[31] V. Krachmalnicoff, J.-C. Jaskula, M. Bonneau, V. Leung, G. B. Partridge, D. Boiron, C. I. Westbrook, P. Deuar, P. Ziń, M. Trippenbach, and K. V. Kheruntsyan, Phys. Rev. Lett. **104**, 150402 (2010).
[32] P. Deuar, J.-C. Jaskula, M. Bonneau, V. Krachmalnicoff, D. Boiron, C. I. Westbrook, and K. V. Kheruntsyan, Phys. Rev. A **90**, 033613 (2014).
[33] R. J. Lewis-Swan, *Ultracold Atoms for Foundational Tests of Quantum Mechanics* (Springer International Publishing, New York, 2016).
[34] R. Bach, M. Trippenbach, and K. Rzążewski, Phys. Rev. A **65**, 063605 (2002).
[35] J. Chwedeńczuk, P. Ziń, M. Trippenbach, A. Perrin, V. Leung, D. Boiron, and C. I. Westbrook, Phys. Rev. A **78**, 053605 (2008).
[36] R. Dall and A. Truscott, Opt. Commun. **270**, 255 (2007).
[37] A. G. Manning, R. I. Khakimov, R. G. Dall, and A. G. Truscott, Nat. Phys. **11**, 539 (2015).
[38] P. L. Kapitza and P. A. M. Dirac, Math. Proc. Cambridge Philos. Soc. **29**, 297 (1933).
[39] P. L. Gould, G. A. Ruff, and D. E. Pritchard, Phys. Rev. Lett. **56**, 827 (1986).
[40] Y. B. Ovchinnikov, J. H. Müller, M. R. Doery, E. J. D. Vredenbregt, K. Helmerson, S. L. Rolston, and W. D. Phillips, Phys. Rev. Lett. **83**, 284 (1999).
[41] P. Deuar, T. Wasak, P. Ziń, J. Chwedeńczuk, and M. Trippenbach, Phys. Rev. A **88**, 013617 (2013).
[42] F. Zambelli, L. Pitaevskii, D. M. Stamper-Kurn, and S. Stringari, Phys. Rev. A **61**, 063608 (2000).
[43] S. S. Hodgman, R. G. Dall, A. G. Manning, K. G. H. Baldwin, and A. G. Truscott, Science **331**, 1046 (2011).
[44] A. S. Campbell, D. M. Gangardt, and K. V. Kheruntsyan, Phys. Rev. Lett. **114**, 125302 (2015).
[45] C. K. Hong, Z. Y. Ou, and L. Mandel, Phys. Rev. Lett. **59**, 2044 (1987).
[46] K. V. Kheruntsyan and P. D. Drummond, Phys. Rev. A **66**, 031602 (2002).
[47] Since the halo density is low enough and the *s*-wave interactions among the halo atoms are minimal, and therefore, the expansion can be assumed to be ballistic.
[48] W. S. Bakr, J. I. Gillen, A. Peng, S. Fölling, and M. Greiner, Nature (London) **462**, 74 (2009).
[49] J. F. Sherson, C. Weitenberg, M. Endres, M. Cheneau, I. Bloch, and S. Kuhr, Nature (London) **467**, 68 (2010).
[50] M. Cheneau, P. Barmettler, D. Poletti, M. Endres, P. Schauß, T. Fukuhara, C. Gross, I. Bloch, C. Kollath, and S. Kuhr, Nature (London) **481**, 484 (2012).
[51] L. W. Cheuk, M. A. Nichols, M. Okan, T. Gersdorf, V. V. Ramasesh, W. S. Bakr, T. Lompe, and M. W. Zwierlein, Phys. Rev. Lett. **114**, 193001 (2015).
[52] E. Haller, J. Hudson, A. Kelly, D. A. Cotta, B. Peaudecerf, G. D. Bruce, and S. Kuhr, Nat. Phys. **11**, 738 (2015).
[53] A. Omran, M. Boll, T. A. Hilker, K. Kleinlein, G. Salomon, I. Bloch, and C. Gross, Phys. Rev. Lett. **115**, 263001 (2015).
[54] B. J. Lester, N. Luick, A. M. Kaufman, C. M. Reynolds, and C. A. Regal, Phys. Rev. Lett. **115**, 073003 (2015).
[55] W. Vassen, C. Cohen-Tannoudji, M. Leduc, D. Boiron, C. I. Westbrook, A. Truscott, K. Baldwin, G. Birkl, P. Cancio, and M. Trippenbach, Rev. Mod. Phys. **84**, 175 (2012).
[56] A. Perrin, C. M. Savage, D. Boiron, V. Krachmalnicoff, C. I. Westbrook, and K. V. Kheruntsyan, New J. Phys. **10**, 045021 (2008).
[57] K. V. Kheruntsyan, M. K. Olsen, and P. D. Drummond, Phys. Rev. Lett. **95**, 150405 (2005).
[58] R. J. Lewis-Swan and K. V. Kheruntsyan, Phys. Rev. A **91**, 052114 (2015).
[59] K. F. Lee, J. Chen, C. Liang, X. Li, P. L. Voss, and P. Kumar, Opt. Lett. **31**, 1905 (2006).
[60] K. He, I. I. Satija, C. W. Clark, A. M. Rey, and M. Rigol, Phys. Rev. A **85**, 013617 (2012).
[61] A. M. Rey, R. Sensarma, S. Fölling, M. Greiner, E. Demler, and M. D. Lukin, Europhys. Lett. **87**, 60001 (2009).
[62] M. Kunitski, S. Zeller, J. Voigtsberger, A. Kalinin, L. P. H. Schmidt, M. Schöffler, A. Czasch, W. Schöllkopf, R. E. Grisenti, T. Jahnke, D. Blume, and R. Dörner, Science **348**, 551 (2015).